

THE FIRST NAKED-EYE SUPERFLARE DETECTED FROM PROXIMA CENTAURI

WARD S. HOWARD¹, MATT A. TILLEY², HANK CORBETT¹, ALLISON YOUNGBLOOD³, R. O. PARKE LOYD^{4,5}, JEFFREY K. RATZLOFF¹, OCTAVI FORS^{1,6}, DANIEL DEL SER^{1,6}, EVGENYA L. SHKOLNIK⁷, CARL ZIEGLER¹, ERIN E. GOEKE¹, AARON D. PIETRAALLO¹, JOSHUA HAISLIP¹, NICHOLAS M. LAW¹*Draft version December 3, 2024*

ABSTRACT

Proxima b is a terrestrial-mass planet in the habitable-zone of Proxima Centauri. Proxima Centauri's high stellar activity however casts doubt on the habitability of Proxima b: sufficiently bright and frequent flares and any associated proton events may destroy the planet's ozone layer, allowing lethal levels of UV flux to reach its surface. In March 2016, the Evryscope observed the first naked-eye-visible superflare detected from Proxima Centauri. Proxima increased in brightness by a factor of ~ 68 during the superflare and released a bolometric energy of $10^{33.5}$ erg, $\sim 10\times$ larger than any previously-detected flare from Proxima. Over the last two years the Evryscope has recorded 23 other large Proxima flares ranging in bolometric energy from $10^{30.6}$ erg to $10^{32.4}$ erg; coupling those rates with the single superflare detection, we predict at least five superflares occur each year. Simultaneous high-resolution HARPS spectroscopy during the Evryscope superflare constrains the superflare's UV spectrum and any associated coronal mass ejections. We use these results and the Evryscope flare rates to model the photochemical effects of NO_x atmospheric species generated by particle events from this extreme stellar activity, and show that the repeated flaring is sufficient to reduce the ozone of an Earth-like atmosphere by 90% within five years. We estimate complete depletion occurs within several hundred kyr. The UV light produced by the Evryscope superflare therefore reached the surface with $\sim 100\times$ the intensity required to kill simple UV-hardy microorganisms, suggesting that life would struggle to survive in the areas of Proxima b exposed to these flares.

Keywords: planets and satellites: terrestrial planets, stars: flare, ultraviolet: planetary systems, ultraviolet: stars, surveys

1. INTRODUCTION

The small and cool star Proxima Centauri (hereafter Proxima) hosts Proxima b, a likely rocky planet (Anglada-Escudé et al. 2016; Bixel & Apai 2017) within the habitable zone (e.g. Meadows et al. 2016; Ribas et al. 2016). Proxima b has potential difficulties in maintaining a habitable atmosphere, both due to possible tidal locking (Grießmeier et al. 2009) and incident stellar activity (e.g. Tarter et al. 2007; Scalo et al. 2007; Seager & Deming 2010; Shields et al. 2016; Davenport et al. 2016).

Proxima is well-known to exhibit large stellar variability and to produce bright flare events. Superflares, extreme stellar events with an estimated bolometric energy release of at least 10^{33} erg (Segura et al. 2010; Tilley et al. 2017; Loyd et al. in prep.), would be one of the largest potential threats to the habitability of Proxima b (Davenport et al. 2016): while ozone in an Earth-like

planet's atmosphere can shield the planet from the intense UV flux associated with a single superflare (Segura et al. 2010; Grießmeier et al. 2016; Tabataba-Vakili et al. 2016), the atmospheric ozone recovery time after a superflare is on the order of years (Tilley et al. 2017). A sufficiently high flare rate can therefore permanently prevent the formation of a protective ozone layer, leading to UV radiation levels on the surface which are beyond what some of the hardiest-known organisms can survive (Grießmeier et al. 2016). The cumulative effect of X-ray and UV flux from both stellar flares and quiescent emission can even strip planetary atmospheres over the course of several Gyr (Cuntz & Guinan 2016; Owen & Mohanty 2016).

Many previous studies have explored low- and moderate-energy flare events on Proxima. Optical surveys have found events with detected energies up to $10^{31.5}$ erg (10^{32} erg bolometric) in visible light (Davenport et al. 2016). ALMA recently detected a large sub-mm flare (10^{28} erg in ALMA's Band 6), although multiwavelength flare studies are needed to determine how large sub-mm flares relate to flares in other bands and their habitability effects (MacGregor et al. 2018). In the X-ray, events up to 10^{32} erg ($10^{32.7}$ erg bolometric) have been detected (Güdel et al. 2004).

The MOST satellite (Walker et al. 2003) performed the most comprehensive previous measurement of the Proxima flare rate. MOST observed Proxima for 37.6 days, observing 66 white-light flare events, the largest of which was $10^{31.5}$ erg in the MOST band-pass (~ 4500 – 7500 Å). No superflares were observed; extrapolating the cu-

* E-mail: wshoward@unc.edu

¹ Department of Physics and Astronomy, University of North Carolina at Chapel Hill, Chapel Hill, NC 27599-3255, USA

² Dept. of Earth & Space Sciences, University of Washington, Seattle, WA, USA

³ NASA Goddard Space Flight Center, Greenbelt, MD, 20771, USA

⁴ Laboratory for Atmospheric and Space Physics, University of Colorado, 600 UCB, Boulder, CO 80309, USA

⁵ Department of Astrophysical and Planetary Sciences, University of Colorado, 2000 Colorado Ave, Boulder, CO 80305, USA

⁶ Institut de Ciències del Cosmos (ICCUB), Universitat de Barcelona, IEEC-UB, Martí i Franquès 1, E08028 Barcelona, Spain

⁷ School of Earth and Space Exploration, Arizona State University, Tempe, AZ, 85282, USA

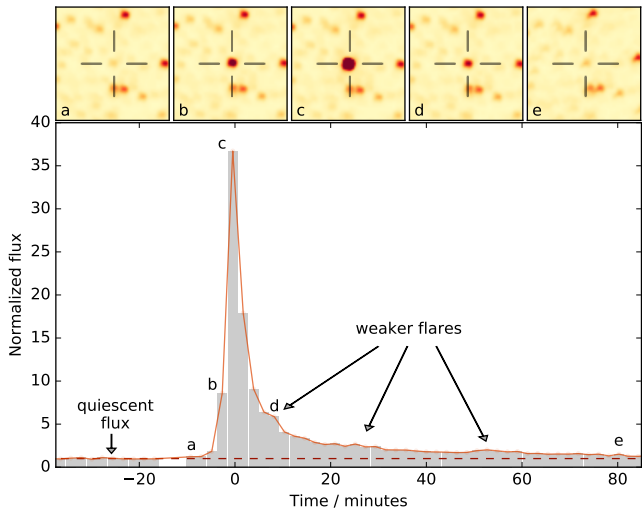


Figure 1. The Evryscope discovery of a naked-eye-brightness superflare from Proxima. The x-axis is time in minutes compared to the flare peak emission time; the y-axis is the flux increase over Proxima’s median g' -band flux from the previous hour. Bars show the integration time of each individual flux measurement. Insets display cutout images over the course of the flare at the times noted on the light curve. For clarity, we here show only one camera’s light curve; another Evryscope camera simultaneously observing the event showed a very similar light curve offset by 2.2 seconds.

mulative flare frequency distribution (FFD) obtained by Davenport et al. (2016) from the MOST flare sample out by 1.5 dex predicts $\sim 8 \times 10^{33+}$ erg events in the MOST bandpass occur per year.

To search for superflares and other short-timescale phenomena, the Evryscope (Law et al. 2015) is performing long-term high-cadence monitoring of Proxima, along with every other bright star in the Southern sky. In March 2016 the Evryscope detected the first-known Proxima superflare. The superflare had a bolometric energy of $10^{33.5}$ erg, $\sim 10\times$ larger than any previously-detected flare from Proxima, and $30\times$ larger than any optically-measured Proxima flare. The event briefly increased Proxima’s visible-light emission by a factor of $38\times$ averaged over the Evryscope’s 2-minute cadence, or $\sim 68\times$ at the cadence of the human eye. Although no M-dwarfs are usually visible to the naked-eye (e.g., Shields et al. 2016), Proxima briefly became a magnitude-6.8 star during this superflare, visible to dark-site naked-eye observers.

2. EVRYSCOPE FLARE DISCOVERY AND OBSERVATIONS

We discovered the Proxima superflare as part of the Evryscope survey of all bright Southern stars. The Evryscope is an array of small telescopes simultaneously imaging 8000 square degrees of the sky every two minutes (Law et al. 2015). The Evryscope observes essentially the entire Southern sky above an airmass of two, at two-minute cadence in g' and at a resolution of $13''\text{pixel}^{-1}$. The system has a typical dark-sky limiting magnitude of $g'=16$ and tracks the sky for 2 hours at a time before ratcheting back and continuing observations, for an average of ~ 6 hours of continuous monitoring each night on each part of the sky.

The Evryscope image archive contains 2.5 million raw images, $\sim 350\text{TB}$ of data. A custom pipeline analyzes the Evryscope dataset at realtime rates (Law et al.

2016). Each image, consisting of a 30 MPix FITS file from one camera, is calibrated using a custom wide-field solver. After careful background modeling and subtraction, forced-aperture photometry is extracted based on known source positions in a reference catalog. Light curves are then generated for approximately 15 million sources across the Southern sky by differential photometry in small sky regions using carefully-selected reference stars and a range of aperture sizes; residual systematics are removed using two iterations of the SysRem detrending algorithm. In extremely crowded fields, such as for Proxima (-2° galactic latitude), we re-run the pipeline for particular targets, optimizing the aperture sizes to avoid nearby stars.

As a very large event, the Proxima Superflare was discovered in routine by-eye checks of interesting targets in the Evryscope data set. Smaller flares are discovered and characterized with an automated flare-analysis pipeline which uses a custom flare-search algorithm, including injection tests to measure the flare recovery rate. First, we search for flares by attempting to fit an exponential-decay matched-filter similar to that of Liang et al. (2016) to each contiguous segment of the Evryscope light curve. Matches with a significance greater than 2.5σ are verified by eye. The entire Proxima lightcurve is also visually examined for flares to account for false-negatives in the automated search.

The fractional flux and equivalent duration (ED) for each flare are calculated as described in Hawley et al. (2014), and flare start and stop times are initially chosen where the flare candidate exceeds the local noise and are subsequently confirmed or adjusted by eye. We inject simulated flares separately into each light curve and perform 20 trials of randomly-located flare injection and attempted recovery per contiguous lightcurve segment. We average the results across the lightcurve to measure recovery completeness as a global function of flare contrast and ED and to quantify the error in contrast and ED for each detected flare.

2.1. Simultaneous high-resolution spectra from HARPS

The superflare reported here occurred during the three-month *Pale Red Dot* campaign, which first revealed the presence of Proxima b (Anglada-Escudé et al. 2016) using the HARPS spectrograph on the ESO 3.6m at La Silla, Chile (Mayor et al. 2003). The HARPS spectrum was taken at 2016 March 18 8:59 UT, 27 minutes after the flare peak at 8:32 UT. This single 1200 second exposure captured the majority of the tail of the flare, including 20% of the total radiated flux.

3. PROXIMA SUPERFLARE PROPERTIES

The Evryscope detected a very large flare from Proxima on 2016 March 18, 8:32:10 UT (MJD 57465.35568, see Figure 1). The flare lasted approximately one hour, with the bulk of the emission occurring in less than 10 minutes during the flare peak. The flare energy release was dominated by a single large event but subsequently showed a complex morphology, with three weaker flares (each more than doubling Proxima’s g' -band brightness) following within an hour.

3.1. Peak brightness

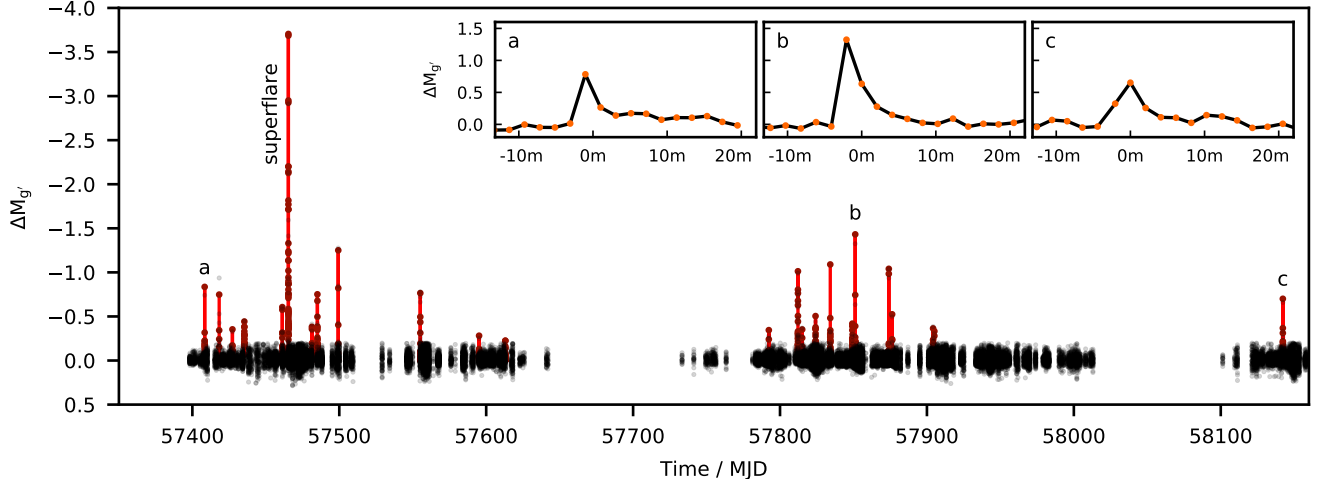


Figure 2. The full 2016-18 Evryscope Proxima light curve. Detected flares are highlighted in red; to show short-term activity Proxima’s long-term variability has been removed from the light curve. The superflare is 2.5-magnitudes brighter than any other Evryscope-detected flare from Proxima. For clarity, we plot only 20% of the 40,486 light curve points. Three representative flares are shown in detail. Because of the two-minute sampling, low-energy, short flares such as the rightmost individually-displayed flare often do not show classical rapid-rise flare shapes, although low-significance flare events are often confirmed with observations from multiple cameras simultaneously.

Within the Evryscope’s two-minute integration during the flare peak, Proxima reached an average flux of $38\times$ the quiescent emission. By fitting a canonical instantaneous-flux flare template (Davenport et al. 2014) to our data, accounting for the two-minute integration time of each measured datapoint, we estimate the superflare’s brightness on human-eye timescales to have reached $68\times$ Proxima’s flux. Proxima, an 11.4 g' magnitude star, thus briefly became a star with a g' magnitude of 6.8, visible to observers at very dark sites (Weaver 1947).¹

3.2. Energy release and planetary-impact-relevant fluxes

Calculation of the superflare’s atmospheric impacts requires an estimate of the flare’s energy in multiple bandpasses, from the far-UV to the infrared. We measure the superflare energy in the g' Evryscope bandpass and subsequently convert into the bolometric flare energy using the energy partitions of Osten & Wolk (2015): we accomplish this by estimating the bolometric flare energy of a 9000 K flare blackbody with emission matching the measured Evryscope flux; the fraction of the bolometric energy found in the Evryscope g' bandpass is $f_{g'}=0.19$. The canonical value of 9000 K provides a lower limit to the flare energy; a higher-temperature flare blackbody, as has been sometimes measured for larger flares (Kowalski et al. 2010) results in more short-wavelength energy than we report. The superflare energy seen in any bandpass $\Delta\lambda$ is then given by the approximate relationship $E_{\Delta\lambda} = f_{\Delta\lambda} \times E_{\text{bol}}$.

We obtain the quiescent flux in the Evryscope g' bandpass by scaling directly from the Evryscope-measured calibrated magnitude, and by weighting the flux-calibrated spectrum of Proxima used in Davenport et al. (2016) by the Evryscope response function and scaling using Proxima’s distance (Lurie et al. 2014). Both methods measure Proxima’s quiescent flux in the

Evryscope bandpass to be $L_0 = 10^{28.6}$ erg per second, giving the superflare’s energy in the Evryscope bandpass of $10^{32.8}$ erg, and a total bolometric energy release of $10^{33.5}$ erg.

3.3. Proxima’s flare frequency distribution

The Evryscope observed Proxima for a total of 1344 hours between January 2016 and March 2018. We discovered 24 large flares (Figure 2), with bolometric energies ranging from $10^{30.6}$ erg to $10^{33.5}$ erg. To estimate the rate of flares of particular energies (the cumulative flare frequency distribution, FFD), we calculate the uncertainty in the cumulative occurrence rate for each Evryscope flare with a binomial 1σ confidence interval statistic (following Davenport et al. 2016). Errors in energy for high-energy flares are calculated using the inverse significance of detection; low-significance flares use the injection-and-recovery error estimate instead, to account for the possibility of correlated noise introducing bias.

To sample both the rare high-energy events detectable by Evryscope and the frequent low-energy events detectable by MOST, we also include flares from the MOST sample (Davenport et al. 2016) with energy in the MOST bandpass greater than $10^{30.5}$ erg. We fit a cumulative power-law FFD to the MOST and Evryscope flares, and determine the uncertainty in our fit through 10,000 Monte-Carlo posterior draws consistent with our uncertainties in energy and occurrence rates. We represent the cumulative FFD in the Evryscope bandpass (Figure 3) by a power law of the form $\log \nu = (1-\alpha) \log E + b$, where ν is the number of flares with an energy greater than or equal to E erg per day, α gives the frequency at which flares of various energies occur, and b is the y-intercept and crossover into the unphysical energy region $E < 0$.

Evryscope constrains the expected occurrence of 10^{33} erg superflares to be at least $5.2^{+0.2}_{-3.0}$ per year. It is evident from Figure 3 that it is difficult to fit a single power law which reproduces both the lower-energy flares and the Evryscope-observed superflare at reasonable proba-

¹ Proxima also reached $V=6.8$ during the flare, as the 0.2 magnitude reduction in flare contrast is offset by the 0.2 magnitude increase to Proxima’s quiescent brightness in V .

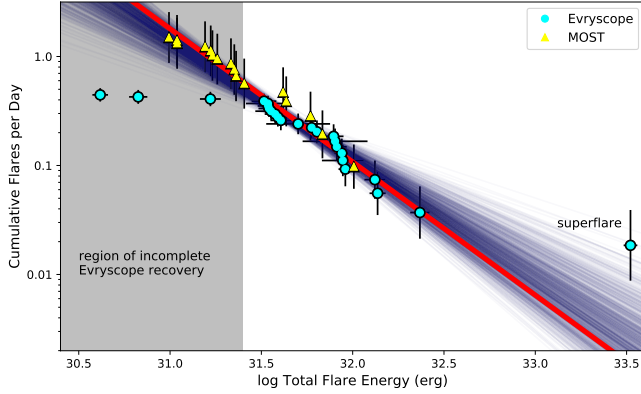


Figure 3. The cumulative flare frequency distribution of Proxima fit to all Evryscope flares and the largest MOST flares, scaled to bolometric energy from the g' and MOST bandpass, respectively. The best fit, which excludes the naked-eye superflare, is displayed in red. 10,000 posterior draws (1000 shown) estimate the error of this power-law fit.

bility. This could mean the probability of reaching superflare energies is higher than would be expected by a simple power-law extrapolation from lower energies; it could also be that the Proxima Superflare is just a rare event. We therefore report two separate FFDs; the first excludes the Proxima Superflare, while the second includes it. For the no-superflare case, we report an FFD of $\log \nu = -1.22^{+0.26}_{-0.003} \log E + 38.1^{+8.4}_{-0.07}$, displayed in Figure 3, in good agreement with both the Evryscope and MOST sample. Including the prior of the observed superflare, we obtain $\log \nu = -0.98^{+0.02}_{-0.24} \log E + 30.6^{+0.83}_{-7.6}$. We note $\alpha_{\text{Evryscope}}$ is significantly steeper in our higher-energy flare sample in both cases than that for Proxima FFDs from previous studies, e.g. Walker (1981); Davenport et al. (2016).

3.4. High-resolution flare spectrum

The mean-subtracted spectrum of Proxima, in both the median quiescent and flare states, is shown in Figure 4. During the superflare, chromospheric metals and the Balmer series show sharply increased emission. A -30 km s^{-1} splitting of the H_α , H_β , and He I lines is detectable, and is indicative of a flow of highly ionized plasma generated by the flare, most likely correlated to a hot stellar wind moving outwards from the star (Pavlenko et al. 2017). No significantly blueshifted emission or anomalous emission lines are visible; the superflare spectrum is similar to other smaller flares recorded from Proxima and is therefore likely to be amenable to emission-line scaling relations to estimate FUV and particle fluxes (Section 3.5).

3.5. UV and particle fluxes

Far-UV (FUV; 100–912 Å) photons are of particular importance to planetary atmospheres as they are capable of photolyzing most molecules. The *Hubble Space Telescope* archive contains 13.3 h of FUV spectrophotometry by the STIS spectrograph of Proxima. From this data, we aggregated 9 flares spanning FUV energies of $10^{29.3} - 10^{30.8}$ erg to construct a characteristic FUV energy budget for Proxima flares. This was scaled to a 9000 K blackbody and EUV emission via a “fiducial flare” prescription (Lloyd et al. in prep.), tailored to

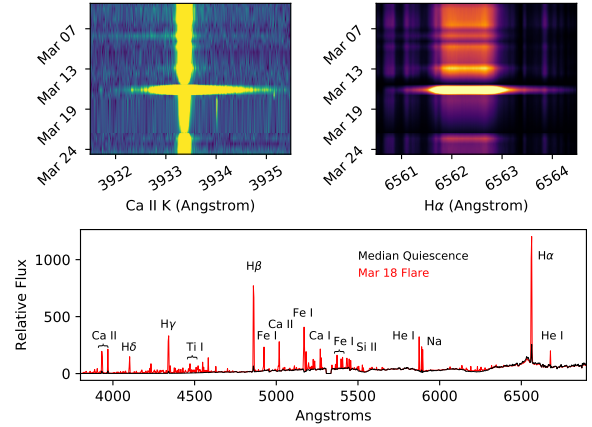


Figure 4. *Top:* Chromospheric activity evolution traced by the Ca II (K) and H_α indicators in the month leading up to the flare. *Bottom:* Mean-flux-subtracted quiescent spectrum (black) and active (red) spectrum 27 minutes after the superflare peak detected by Evryscope. The quiescent Proxima spectrum is a median of the daily spectra from the month leading up to the superflare, reducing the impact of stellar activity features and flares below the photometric detection threshold.

the Proxima data. We independently checked the validity of the fiducial flare prescription used to derive these estimates using the quiescent scaling relations of Youngblood et al. (2017) applied to a measurement of the Ca II K equivalent width in the HARPS spectrum (Section 2.1) and found agreement within the uncertainties, supporting the fiducial FUV superflare energy of $10^{32.5}$ erg.

Coronal mass ejections (CMEs) are often assumed to accompany large flares (e.g., Aarnio et al. 2011; Drake et al. 2013). Youngblood et al. (2017) measures a relation for predicting $>10 \text{ MeV}$ proton fluxes based on the energy of the flare in Si IV. These particles can initiate nonthermal chemical reactions in the planetary atmosphere. From the Youngblood et al. (2017) relation and the HARPS spectrum, we estimate a proton fluence at Proxima b’s 0.0485 AU distance of $10^{6.6}$ protons $\text{cm}^{-2} \text{sr}^{-1}$.

4. ASTROBIOLOGICAL IMPACT OF THE SUPERFLARE

4.1. Demise of the Ozone Column

We employ a 1D coupled, photochemical and radiative-convective climate model to determine the effects of the observed flare activity on the potential habitability of Proxima b. We assume the planet to have an Earth-like atmosphere. The details of the coupled model can be found in Segura et al. (2010) and Tilley et al. (2017), which discovered that the results of only electromagnetic flaring cannot significantly drive O_3 column loss, while flares with proton events can rapidly destroy the O_3 column, with the effects persisting for long periods of time. Proton events lead to the dissociation of N_2 in the planet atmosphere into constituent, excited N-atoms, which then react with O_2 to produce NO and O. NO reacts with O_3 to produce NO_2 . The NO_x species generated during the proton events therefore drive the evolution of the ozone column (see Tilley et al. 2017 for further details).

Using the cumulative flare frequency distribution mea-

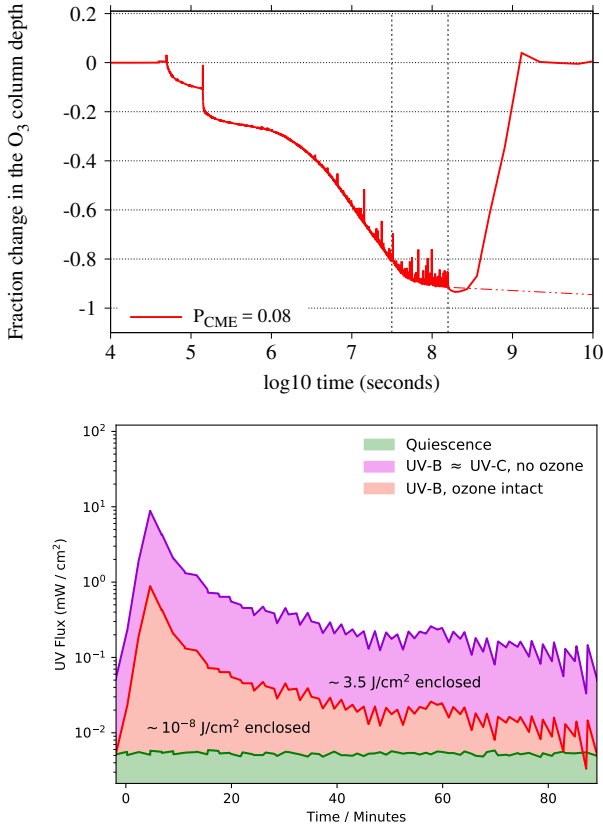


Figure 5. Top panel: The solid red line represents the evolution of the O₃ column for a planet with an Earth-like atmosphere orbiting Proxima Centauri. The vertical lines represent the one year and five year points, and the dash-dotted red line is a projection of future O₃ evolution. Beyond the 5 years, the dash-dotted projection assumes continued flare activity after 5 years; the solid red line assumes no further activity impacts the atmosphere after 5 years and hence returns to Earth-like conditions. Bottom panel: Surface UV-B and UV-C flux during the superflare. Surface flux is calculated as the flux of Proxima during the superflare at the orbit of the planet, with no atmospheric attenuation due to atmospheric volatiles (purple), and an Earth-like, intact ozone column (i.e. only 10% of the top-of-atmosphere UV-B reaches the surface; displayed in red). The no-volatiles UV surface levels during the superflare result in 30× germicidal doses.

sured in the present work and the scaling from Hawley et al. (2014), we generated a sequence of flares for a 5-year time span in the U-band energy range from 10^{29.5} erg to 10^{32.9} erg (scaled to represent the Evryscope-measured flare frequency distribution). Flux stacking is allowed, which can result in complex events. This flare sequence is used to drive the Earth-like atmosphere of a planet in orbit around an active M dwarf star at 0.0485 AU. Flare events are selected at random to produce a proton event, with proton flux scaling with event amplitude. The probability for each flare to generate a planet-oriented energetic particle event is $P = 0.08$, following Tilley et al. (2017) with moderate values for proton event geometries.

The evolution of the O₃ column as a result of the impacting flares and proton events is shown in the top panel of Figure 5. At the end of the five years of flare simulation, 846 of 10,724 flares had generated a proton event that impacted the atmosphere of the planet, resulting in an O₃ column loss of 90%. The system does not appear to reach steady state, instead slowly decreasing the

amount of O₃ with increasing time. We assess that it is likely that Proxima b has suffered extreme ozone loss. At Proxima’s current activity rate, >99.9% of Proxima b’s O₃ is likely to be lost within 100s of kyr, leaving the planet’s surface largely unprotected from UV light.

A complete lack of O₃ would particularly affect the amount of germicidal UV-C reaching the surface. Although other volatiles capable of absorbing UV-C (i.e., O₂, H₂O) are not destroyed at the same rate as ozone, these volatiles do not effectively block UV-C for wavelengths longer than ~2500 Å. No significant Earth-like atmospheric gas but O₃ (i.e. Hartley bands) effectively absorbs in the UV-B and UV-C wavelengths ~2450-2800 Å (Tilley et al. 2017). During the Proxima superflare, the top-of-atmosphere receives ~3.5 J cm⁻² of UV-C in the wavelength range 2400-2800 Å. Absent ozone, most of this radiation reaches the surface. These wavelengths are sufficiently energetic to serve as a germicidal source: for example, most mercury-based lamps are at 2537 Å for germicidal purposes (e.g., Chang et al. 2007), and germicidal LED lamps are 2500 Å and up (e.g., Chatterley & Linden 2010).

4.2. Effects on surface life

Figure 5 shows the UV-B and UV-C flux at the surface of Proxima b during the superflare, given the g' flux measured in the Evryscope light curve, the flare spectral modeling in Section 3.2, and assuming an orbital radius of 0.0485 AU (Anglada-Escudé et al. 2016). We plot two flare regimes: 1) the expected fluxes for an intact Earth-like ozone layer (where essentially no UVC reaches the surface, and ~10% of UVB reaches the surface; Grant & Heisler 1997 and references therein); and 2) an extreme ozone-loss scenario, where UVC reaches the surface unimpeded by ozone or other atmospheric absorption (see Section 4), resulting in UV-B≈UV-C surface fluxes (this equivalence is coincidental: the lack of ~2500 Å UV-C reaching the surface counters the proximity to the flare blackbody peak). We assume cloudless skies.

While UV-B accounts for only 5% of the solar UV radiation incident upon Earth, it has the largest impact upon terrestrial biology because shorter UV-C wavelengths are blocked by ozone in the Earth’s atmosphere (Slinney & Wolbarsht 1980). During the Evryscope superflare, 3.5 J cm⁻² of UV-B reached the surface under the assumption of extreme ozone attenuation, which is below a lethal dose of 4 J cm⁻² for *Deinococcus radiodurans* but lethal for most UV-hardy organisms, even when protected by a shallow layer of freshwater. For example, in the top 50 cm of water, 1.5 J cm⁻² of UV-B will kill 50% of freshwater invertebrates (Hurtubise et al. 1998). Zooplankton receive a lethal dose of UV-B at 0.5 J cm⁻² (Rautio & Korhola 2002).

UV-C radiation is much more efficient at damaging DNA than UV-B (Rehmtulla et al. 1997; Batista et al. 2009). Although *D. radiodurans* is amongst the most UV-resilient organisms on Earth, its UV-C D90 dose (i.e., the amount of radiation required to kill 90% of the population) of 0.0553 J cm⁻² (Gascón et al. 1995) is a factor of 65× smaller than the 3.6 J cm⁻² that reaching the surface during the Proxima Superflare, given no

ozone. Recent results have suggested that some more complex life such as lichens evolved for extreme environments and with adaptations such as UV-screening pigments may survive these radiation levels (Brandt et al. 2015); this suggests that life on Proxima b will have to undergo complex adaptations to survive, even if the planetary atmosphere survives the long-term impact of the stellar activity.

5. CONCLUSIONS

Two-thirds of M-dwarfs are active (West et al. 2015), and superflares will significantly impact the habitability of the planets orbiting many of these stars, which make up the majority of the Galaxy’s stellar population. Measuring the impact of superflares on these worlds will thus be a necessary component in the search for extraterrestrial life on planets discovered by TESS (Ricker et al. 2014) and other surveys. Beyond Proxima, Evryscope has already performed similar long-term high-cadence monitoring of every other Southern TESS planet-search target, and will therefore be able to measure the habitability impact of stellar activity for all Southern planet-search-target M-dwarfs (Howard et al., in prep.). In conjunction with coronal-mass-ejection searches from long-wavelength radio arrays like the LWA (Hallinan & Anderson 2017), the Evryscope will constrain the long-term atmospheric effects of this extreme stellar activity.

On Proxima b, the superflare we detected, along with Proxima’s regular and extreme activity, leads to our photochemical model predicting 90% ozone destruction within 5 years. As Proxima’s ozone column fraction does not appear to reach a steady state at the end of that period but instead continues a clear downward trend, we conclude that Proxima b has likely suffered extreme ozone loss over long timescales. If the current activity rate of Proxima holds for longer timescales, >99.9% of the planetary O₃ is likely to be lost within 100s of kyr, leaving the planet’s surface largely unprotected from UV light, and forcing extreme adaptation by any organisms on the Proxima-facing surface of Proxima b.

ACKNOWLEDGEMENTS

The authors wish to thank James R. Davenport, J.J. Hermes, Bart H. Dunlap, and Joshua Reding for insightful comments. WH, HC, NL, JR, CZ, and EG acknowledge funding support by the National Science Foundation CAREER grant 1555175, and the Research Corporation Scialog grants 23782 and 23822. HC is supported by the National Science Foundation Graduate Research Fellowship under Grant No. DGE-1144081. OF acknowledges funding support by the grant MDM-2014-0369 of the ICCUB (Unidad de Excelencia ‘María de Maeztu’). AY acknowledges support by an appointment to the NASA Postdoctoral Program at Goddard Space Flight Center, administered by URSA through a contract with NASA. R.O.P.L. appreciates support from a STScI grant, HST-GO-14784.001-A (PI Shkolnik). E.L.S. appreciates support from NASA/Habitable Worlds grant NNX16AB62G. The Evryscope was constructed under National Science Foundation/ATI grant AST-1407589.

Facilities: CTIO:Evryscope, HST (STIS), ESO:3.6m (HARPS)

REFERENCES

- Aarnio, A. N., Stassun, K. G., Hughes, W. J., & McGregor, S. L. 2011, *Sol. Phys.*, 268, 195
- Anglada-Escudé, G., Amado, P. J., Barnes, J., et al. 2016, *Nature*, 536, 437
- Batista, L. F., Kaina, B., Meneghini, R., & Menck, C. F. 2009, *Mutation Research/Reviews in Mutation Research*, 681, 197
- Bixel, A., & Apai, D. 2017, *ApJ*, 836, L31
- Brandt, A., de Vera, J.-P., Onofri, S., & Ott, S. 2015, *International Journal of Astrobiology*, 14, 411425
- Chang, C. P., Liu, H. H., Peng, C. Y., Shieh, J. Y., & Lan, C. H. 2007, *Health Phys.*, 92, 242
- Chatterley, C., & Linden, K. 2010, *J Water Health*, 8, 479
- Cuntz, M., & Guinan, E. F. 2016, *ApJ*, 827, 79
- Davenport, J. R. A., Kipping, D. M., Sasselov, D., Matthews, J. M., & Cameron, C. 2016, *ApJ*, 829, L31
- Davenport, J. R. A., Hawley, S. L., Hebb, L., et al. 2014, *ApJ*, 797, 122
- Drake, J. J., Cohen, O., Yashiro, S., & Gopalswamy, N. 2013, *ApJ*, 764, 170
- Gascón, J., Oubiña, A., Pérez-Lezaun, A., & Urmeneta, J. 1995, *Current Microbiology*, 30, 177
- Grant, R. H., & Heisler, M. 1997, *Journal of Applied Meteorology*, 36, 1336
- Grießmeier, J.-M., Stadelmann, A., Grenfell, J. L., Lammer, H., & Motschmann, U. 2009, *Icarus*, 199, 526
- Grießmeier, J.-M., Tabataba-Vakili, F., Stadelmann, A., Grenfell, J. L., & Atri, D. 2016, *A&A*, 587, A159
- Güdel, M., Audard, M., Reale, F., Skinner, S. L., & Linsky, J. L. 2004, *A&A*, 416, 713
- Hallinan, G., & Anderson, M. M. 2017, in *Radio Exploration of Planetary Habitability (AASTCS5)*, Vol. 49, 401.01
- Hawley, S. L., Davenport, J. R. A., Kowalski, A. F., et al. 2014, *ApJ*, 797, 121
- Hurtubise, R. D., Havel, J. E., & Little, E. E. 1998, *Limnology and Oceanography*, 43, 1082
- Kowalski, A. F., Hawley, S. L., Holtzman, J. A., Wisniewski, J. P., & Hilton, E. J. 2010, *ApJ*, 714, L98
- Law, N. M., Fors, O., Ratzloff, J., et al. 2016, in *Proc. SPIE*, Vol. 9906, Ground-based and Airborne Telescopes VI, 99061M
- Law, N. M., Fors, O., Ratzloff, J., et al. 2015, *PASP*, 127, 234
- Liang, E.-S., Wang, S., Zhou, J.-L., et al. 2016, *AJ*, 152, 168
- Loyd, R. O. P., et al. in prep., *ApJ*
- Lurie, J. C., Henry, T. J., Jao, W.-C., et al. 2014, *AJ*, 148, 91
- McGregor, M. A., Weinberger, A. J., Wilner, D. J., Kowalski, A. F., & Cranmer, S. R. 2018, *ApJ*, 855, L2
- Mayor, M., Pepe, F., Queloz, D., et al. 2003, *The Messenger*, 114, 20
- Meadows, V. S., Arney, G. N., Schwieterman, E. W., et al. 2016, *ArXiv e-prints*, arXiv:1608.08620
- Osten, R. A., & Wolk, S. J. 2015, *ApJ*, 809, 79
- Owen, J. E., & Mohanty, S. 2016, *MNRAS*, 459, 4088
- Pavlenko, Y., Suárez Mascareño, A., Rebolo, R., et al. 2017, *A&A*, 606, A49
- Rautio, M., & Korhola, A. 2002, *Polar Biology*, 25, 460
- Rehmtulla, A., Hamilton, C. A., Chinnaiyan, A. M., & Dixit, V. M. 1997, *The Journal of biological chemistry*, 272, 25783
- Ribas, I., Bolmont, E., Selsis, F., et al. 2016, *A&A*, 596, A111
- Ricker, G. R., Winn, J. N., Vanderspek, R., et al. 2014, in *Proc. SPIE*, Vol. 9143, Space Telescopes and Instrumentation 2014: Optical, Infrared, and Millimeter Wave, 914320
- Scalo, J., Kaltenegger, L., Segura, A. G., et al. 2007, *Astrobiology*, 7, 85
- Seager, S., & Deming, D. 2010, *ARA&A*, 48, 631
- Segura, A., Walkowicz, L. M., Meadows, V., Kasting, J., & Hawley, S. 2010, *Astrobiology*, 10, 751
- Shields, A. L., Ballard, S., & Johnson, J. A. 2016, *ArXiv e-prints*, arXiv:1610.05765
- Sliney, D., & Wolbarsht, M. 1980, in *Safety with lasers and other optical sources*, Vol. . (Plenum Press), 194
- Tabataba-Vakili, F., Grenfell, J. L., Grießmeier, J.-M., & Rauer, H. 2016, *A&A*, 585, A96
- Tarter, J. C., Backus, P. R., Mancinelli, R. L., et al. 2007, *Astrobiology*, 7, 30
- Tilley, M. A., Segura, A., Meadows, V. S., Hawley, S., & Davenport, J. 2017, *ArXiv e-prints*, arXiv:1711.08484
- Walker, A. R. 1981, *MNRAS*, 195, 1029

Walker, G., Matthews, J., Kuschnig, R., et al. 2003, PASP, 115,
1023
Weaver, H. F. 1947, PASP, 59, 232

West, A. A., Weisenburger, K. L., Irwin, J., et al. 2015, ApJ, 812,
3
Youngblood, A., France, K., Loyd, R. O. P., et al. 2017, ApJ, 843,
31